Supporting Information

A Vibrating Capillary for Ultrasound Rotation Manipulation of Zebrafish Larvae

Zhiyuan Zhang[a], Yilin Cao[a], Sara Caviglia[b], Prajwal Agrawal[a], Stephan C. F. Neuhauss[b], and Daniel Ahmed*[a]

This document contains the Supplemental Material for the article titled "A Vibrating Capillary for Ultrasound Rotation Manipulation of Zebrafish Larvae ".

*To whom correspondence should be addressed:

dahmed@ethz.ch;

Supporting Note

Acoustic forces get significant on a small scale and are dependent on various factors that affect the scattering of sound waves, such as orientation, size, shape, material properties of the subject and medium, etc. In this work, the acoustic forces acting on the zebrafish larvae can be given as a surface integral of the time-averaged second-order acoustic pressure and the momentum flux tensor at its surface S_0

$$F_A = -\int_{S_0} [\langle p_2 \rangle n + \rho_0 \langle (n \cdot v_1) v_1 \rangle] \, dS$$
$$= -\int_{S_0} \left[\left(\frac{1}{2} \frac{1}{\rho_0 c_0^2} \langle p_1^2 \rangle - \frac{1}{2} \rho_0 \langle v_1^2 \rangle \right) n + \rho_0 \langle (n \cdot v_1) v_1 \rangle \right] dS \quad \text{(S1)}$$

where ρ_0 is the density of the liquid, c_0 indicates the speed of sound in the liquid. p_2 represents the pressure with the sub-index referring to the order of perturbation. The vector n symbolizes the vector normal to the surface and v is considered the acoustic velocity field. However, to date, acoustic radiation forces on objects with soft materials and arbitrary shapes are still largely unexplored. Further theories and derivations regarding the acoustic forces are described in supporting references 1-4.

Supporting figures

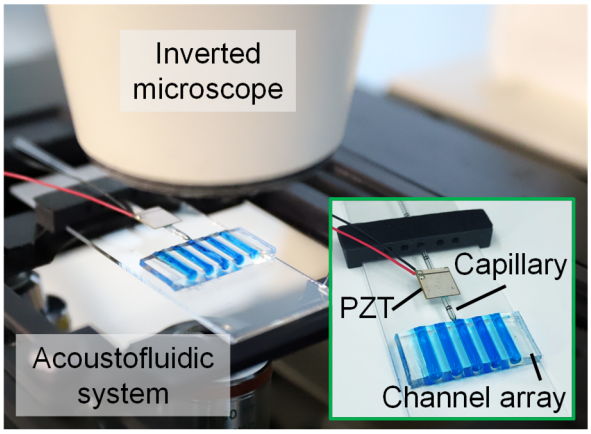

Fig. S1. Experimental setup mounted on an inverted microscope. The channel array is represented by water stained blue.

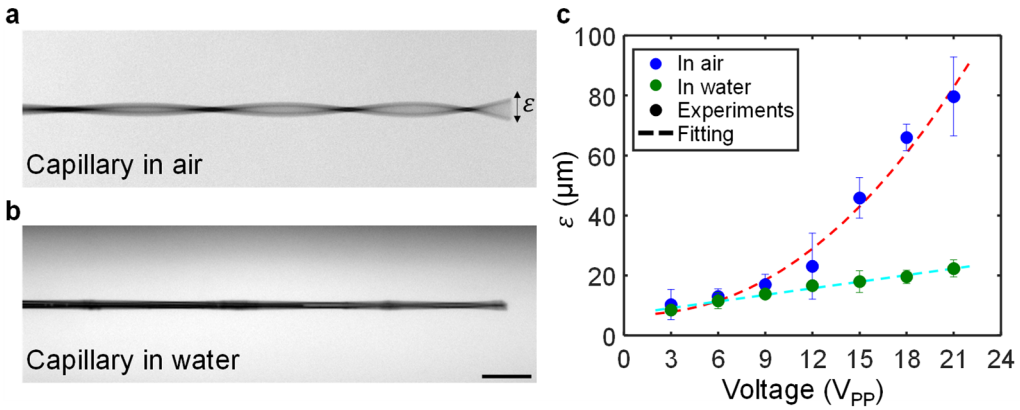

Fig. S2. .Standing wave vibration observed on the glass capillary. a) Capillary vibrates in air. b) Capillary vibrates in water. c) Plots of the vibration amplitude against ultrasound excitation voltage. The data were respectively fitted with a power function of $y = 0.09246x^{2.205} + 6.749$ and a linear function of $y = 0.7346x + 6.904$. The error bars indicate the standard error of the data. The ultrasound excitation frequency was 185 kHz. Scale bar, 100 μm.

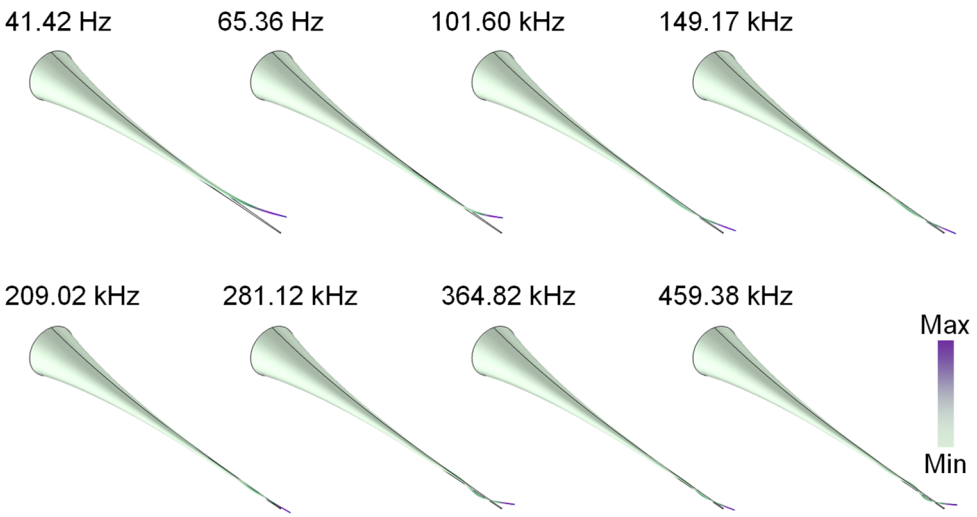

Fig. S3. Simulations of the natural frequency of the utilized glass capillary tip. Eight different orders of the natural frequency were found from 1 Hz to 500 kHz. Errors between the simulation model and the actual system come from the materials, dimensions, boundary conditions, speed of sound and so on. The color bar denotes the vibration amplitude.

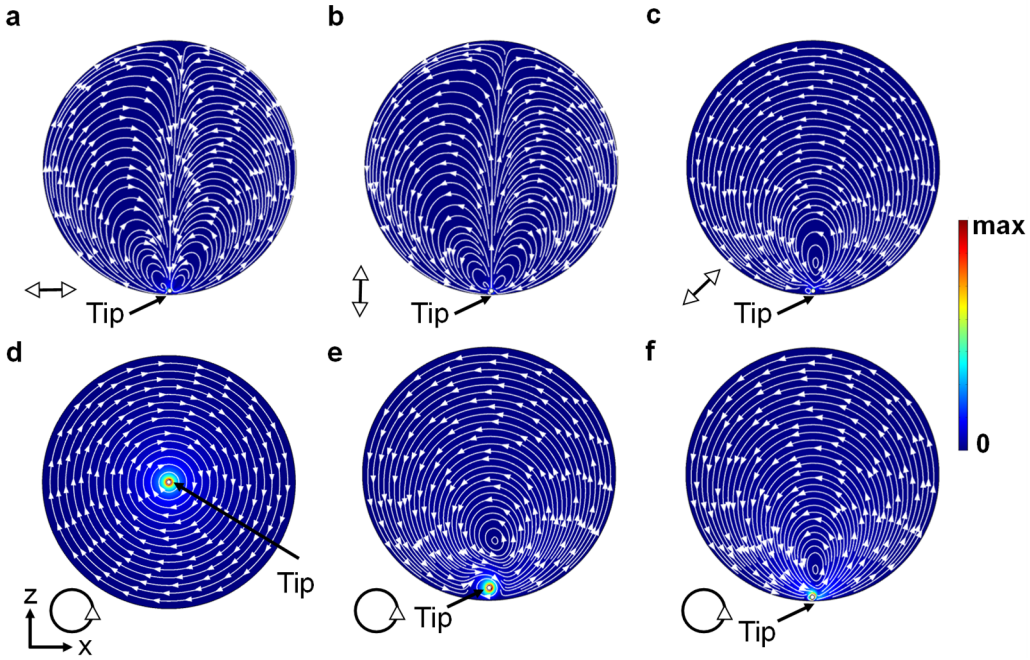

Fig. S4. Simulated flow profiles viewed in cross-section. Flow profile simulation in a) horizontal linear vibrating mode, b) vertical linear vibrating mode, and c) tilted linear vibrating mode with the capillary near the channel boundary. Flow profile simulation in circular vibrating mode with the capillary d) at the channel center, e) around the channel boundary, and f) near the channel boundary. White curves show the developed streaming, while the arrow shows streaming direction and the background color denotes streaming velocity. The vibrating magnitude of the capillary tip was set at 1 nm. Diagrams demonstrate the vibrating mode and direction.

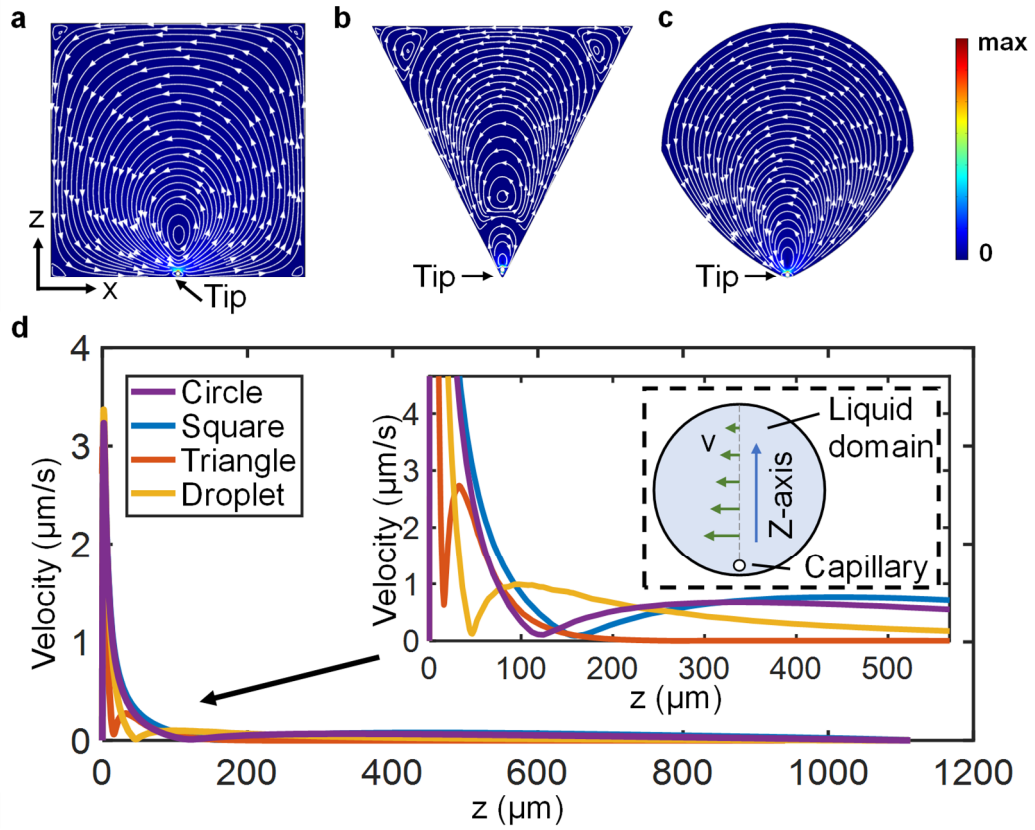

Fig. S5. Simulations of cross-sectional flow profiles in channels with different cross-section shapes. a) – d) Flow profiles in channels with circular, square, triangle, and droplet cross-sections, respectively. White curves show the developed streaming, while the arrow shows streaming direction and the background color denotes streaming velocity. The capillary was placed near the channel boundary. The vibrating mode of the capillary was set as elliptical, and the magnitude as 1 nm. e) Streaming velocity against distance along the z-axis. Inset shows a zoomed-in view of the range 0 – 600 μm.

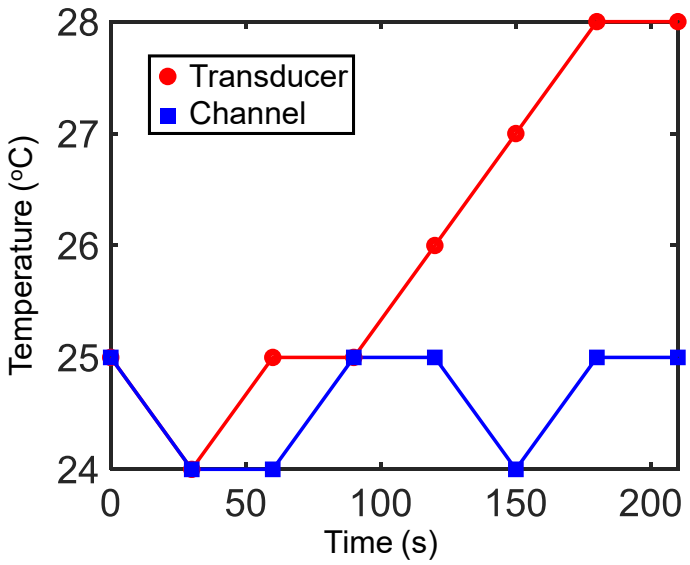

Fig. S6. Plot of local temperature changes against ultrasound excitation time. The ultrasound excitation frequency and voltage were kept at 185 kHz and 20 V_{PP}, respectively. The temperature was measured by using a handheld non-contact laser thermometer with a resolution of 0.1 °C. The laser was vertically aligned to the center of the transducer and the microchannel. The distance between the thermometer detection end and the measured point was kept at a constant at 1 mm. We measured the temperature change before and after the ultrasound excitation in 0—4 minutes with an increment of 30 s.

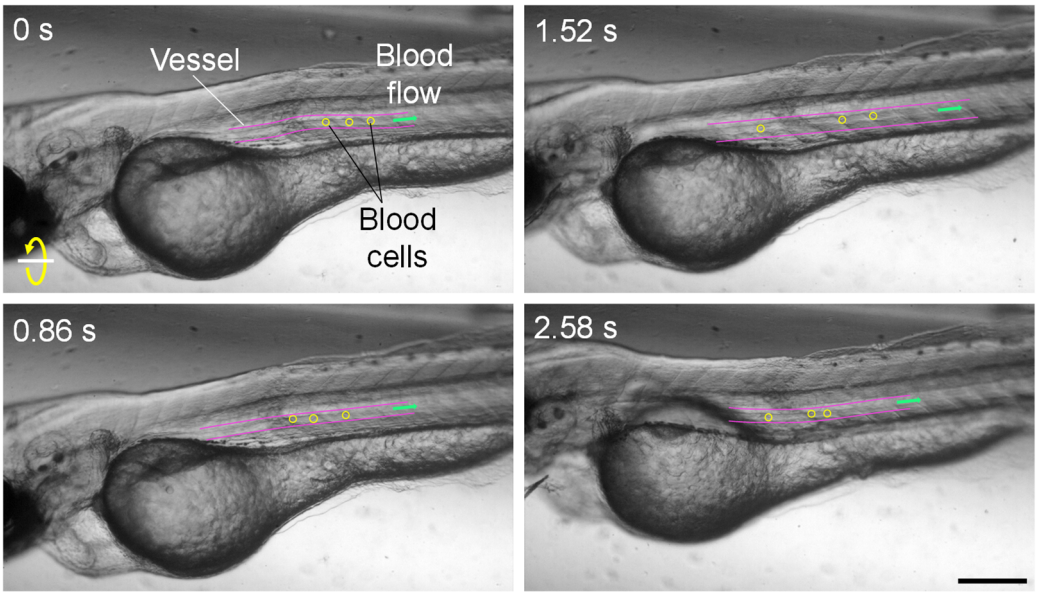

Fig. S7. Image sequence shows the moving blood cells in a rotating zebrafish larva with different rotational angles. The ultrasound excitation frequency and voltage were 185 kHz and 6 V_{PP}, respectively. Yellow circles show the moving single blood cells. These three blood cells were different cells. The green arrow denotes the direction of the blood flow. The magenta lines denote the boundaries of the vessel. Scale bar, 100 µm.

Supporting table

Table S1. The parameters and configuration used in numerical simulations.

Items	**Parameters/type**
Acoustics	Thermoviscous Acoustic, Frequency Domain
Fluidics	Laminar Flow
Material	Water (built-in material of COMSOL)
Wall condition	Non-slip
Radius of the cross-section channel	570 μm
Radius of the capillary	20 μm
Amplitude of vibration	1 nm-10000 nm
Frequency of vibration	185 kHz/ 240 kHz
Model of Vibration	Linear/ elliptical
Volume Force of liquid	F_x = - 0.5*real(conj(ta.rho)*ta.iomega*u)-ta.rho0*0.5*(real(conj(u)*d(u,x))+real(conj(v)*d(u,y))) F_y = -0.5*real(conj(ta.rho)*ta.iomega*v)-ta.rho0*0.5*(real(conj(u)*d(v,x))+real(conj(v)*d(v,y))) (ta.rho0 is the density of water; ta.iomega is the angular frequency of the vibration; *u* and *v* are the velocity components of *x* direction and *y* direction, respectively.)
Mesh	Controlled by physical fields (finer)
Study 1	Frequency domain study of acoustics
Study 2	Stationary study of fluidics

Supporting videos

Video S1. Animation of rotational mechanism.

Video S2. Acoustofluidic behaviors of the vibrating capillary.

Video S3. Cross-section flow profile analysis.

Video S4. Trapping of zebrafish larvae.

Video S5. Rotation of zebrafish larvae.

Video S6. Viability of zebrafish larvae.

Video S7. Rotation of fluorescently labeled zebrafish larvae.

Video S8. 3D reconstruction of a zebrafish larva.

Supporting References

1. T. S. Jerome, Y. A. Ilinskii, E. A. Zabolotskaya, M. F. Hamilton, *J. Acoust. Soc. Am*. **2019**, 145, 1.
2. K. M. Lim, S. S. Rahnama, *Inter. J. Modern Phys. Conf. series* **2014**, 34, 1460380.
3. H. Olsen, H. Wergeland, P. J. Westervelt, *J. Acoust. Soc. Am*. **1958**, 30, 7.
4. G. R. Torr, *Am. J. Phys.* **1984**, 52, 5.